Jordan Journal of Civil Engineering, Volume **18**, No. **3**, **2024**
DOI: https://doi.org/10.14525/JJCE.v18i3.08

Jordan Journal of Civil Engineering

Journal homepage: https://jjce.just.edu.jo

Study on Shear Behavior and Damage Simulation of Masonry Walls Considering the Effect of Long-term Flood Immersion

Chenhu Lu [1),5)]*, ***Chao Wang*** [2)], ***Mengxue Ma*** [3)], ***Daoyong Wang*** [4)], ***Bo Song*** [5)]

[1)] *Institute of Geophysics, China Earthquake Administration, Beijing, 100081, China.*
* *Corresponding Author. E-Mail: luchenhu98@163.com*
[2)] *BYD Auto Industry Company, Limited, Shenzhen, Guangdong Province, 518118, China.*
[3)] *Shandong Electric Power Engineering Consulting Institute Corporation, Limited, Jinan, Shandong Province, 250013, China.*
[4)] *School of Civil Engineering, Shandong University, Jinan, Shandong Province, 250061, China.*
[5)] *School of Civil and Resource Engineering, University of Science and Technology Beijing, Beijing, 100083, China.*

ARTICLE INFO

Article History:
Received: 8/10/2023
Accepted: 24/5/2024

ABSTRACT

Floods can cause masonry buildings to become immersed for a long period of time, which causes the building materials to deteriorate and thus affects the safety performance of the structure. In this study, a long-term-immersed masonry wall was considered as the research object and a cohesive element containing damage evolution was used to simulate the mortar layer, establish a finite-element model of the separated masonry wall and perform numerical loading experiments. Data on crack width variation in the masonry wall was extracted using Python. The effect of a long-term-water-immersion environment on the shear performance of masonry walls was analyzed considering material deterioration. The results show that long-term flooded masonry walls are characterized by low shear capacity and low stiffness and safety reserves cannot be guaranteed. A partially immersed masonry wall is prone to damage from the weak parts and has a high risk coefficient. The macro-damage degree of a masonry wall immersed by a flood is not as serious as that of the original wall in the early stage, but it suddenly increases in the collapse stage and the warning effect of cracks is reduced, which requires special attention in safety assessments.

Keywords: Masonry wall, Crack width, Flood immersion, Failure, Damage grade.

INTRODUCTION

In recent years, floods have frequently occurred in China, exhibiting a wide range and periodicity. There were 38 regional rainstorms in China in 2022 and the direct economic loss caused by flood disasters throughout the year was 128.9 billion yuans. A certain number of flood storage and detention areas have been established in China's major rivers to store excess floodwater in a timely manner and reduce flood peaks.

When flood disasters occur and the flood storage and detention area is activated, some houses experience long-term immersion and scouring because of the flooding, which can damage the durability of building materials and pose potential safety risks. Masonry structure is one of the most common building structures in rural areas of China. Few studies have been conducted on the safety performance of masonry structures considering the combined actions of multiple disasters (Dong et al., 2022). The performance of masonry mortar will directly affect structural safety (Haddad and Shannag, 2008). The seismic vulnerability of masonry structures makes masonry buildings a weak part of disaster prevention and mitigation and this has attracted great attention at the national level (Chen et al., 2021).

Researchers have conducted many experiments to analyze the changes in the mechanical properties of masonry materials after water immersion. Franzoni et al. (2015) explained the changes in the compressive strength and elastic modulus of masonry materials under dry and wet conditions by analyzing the microscopic characteristics of the materials. It was experimentally demonstrated by Sathiparan et al. (2018) that the presence of water plays a crucial role in the deterioration of material properties. The above mentioned research mainly focused on the influence of moisture on the performance of masonry materials from the perspective of material experiments. It is feasible and necessary to apply the experimental results in the literature to the finite-element modeling of masonry walls after long-term immersion.

Researchers have performed finite-element simulations of masonry structures. The method of homogenizing mortar and blocks into one material is applicable to integral masonry structures (Song et al., 2023) and the development of cracks can be determined according to the plastic damage cloud diagram (Kujawa et al., 2020), but it cannot reflect the impact of the deterioration of the specific material performance. The contact method is widely used to simulate masonry joints, but it does not reflect the bonding properties of mortar (Pandey and Bisht, 2014). On this basis, simulating the mortar layer by using the viscous interface model considering the bonding effect and damage characteristics is widespread in the fine modeling of masonry walls (Zhao et al., 2021; Zeng et al., 2021). When the masonry wall is immersed for a long time, the material properties and bonding strength are affected. Therefore, the changes in the relevant parameters should be investigated to simulate the shear performance of immersed masonry walls.

In this study, masonry walls immersed by floods for a long time were considered as research objects. To fully consider the deterioration of the material and bonding strength caused by long-term immersion, a finite-element model of the separated masonry wall was established based on ABQUAS software and a numerical low-cycle loading test was performed to analyze the changes in the mechanical properties and damage state of the wall before and after immersion.

Finite-element Simulation Method for Separated Masonry Wall

Simplified Modeling of Separated Masonry Wall

Masonry materials are connected using blocks and mortar layers. The strength properties of the two materials are significantly different. The mortar layer is weaker and more attention should be paid to it in the seismic analysis of masonry structures. To analyze the crack development and consider the calculation efficiency, in this study, a modeling method described previously (Kong et al., 2012) was used and a single block was combined with the surrounding one-half thickness of the mortar layer into a composite block. The composite block was simulated using a solid element and the mortar layer was simulated using a zero-thickness cohesive element, as shown in Figure 1.

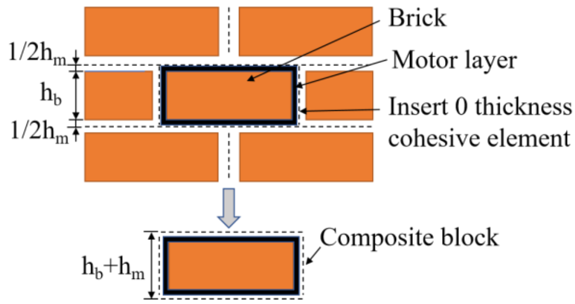

Figure (1): Schematic diagram of composite block

Determination of Constitutive Parameters of Composite Blocks

The Drucker–Prager (DP) model (Drucker and Prager, 1952) is used to simulate composite blocks. It is widely used for friction materials, such as soil and rock and is suitable for simulating materials with compression yield strengths far greater than the tensile yield strength. The DP model requires that the flow stress ratio, expansion angle and friction angle be input and it uses the linear yield criterion. The compressive performance of a block determined using the compressive stress–strain curve was calculated (Kaushik et al., 2007) using Eqs. (1)-(4) in this article. The elastic moduli of the mortar, block and composite block were calculated (Liu et al., 2008) using Eqs. (5)-(7).

$$\frac{f_c}{f_c^{'}} = 2\frac{\varepsilon_c}{\varepsilon_c^{'}} - \left(\frac{\varepsilon_c}{\varepsilon_c^{'}}\right)^2 \quad (1)$$

$$f_c^{'} = 0.63 f_b^{0.49} f_m^{0.32} \quad (2)$$

$$\varepsilon_c^{'} = C_m \frac{f_c^{'}}{E_c^{0.7}} \quad (3)$$

$$C_m = \frac{0.27}{f_m^{0.25}} \quad (4)$$

$$E_b = 4467 f_b^{0.22} \quad (5)$$

$$E_m = 1057 f_m^{0.94} \quad (6)$$

$$E_c = \frac{4467 f_b^{0.22} f_m^{0.84}}{4.226 f_b^{0.22} + f_m^{0.84}} \quad (7)$$

Here, f_c is the compressive strength of brick masonry (MPa); $f_c^{'}$ is the peak compressive strength of brick masonry (MPa); ε_c is the compressive strain of brick masonry; $\varepsilon_c^{'}$ is the peak strain of brick masonry; C_m is the correlation coefficient of mortar compressive strength; f_m is the compressive strength of mortar (MPa); f_b is the compressive strength of the block (MPa); E_m is the elastic modulus of mortar; E_b is the elastic modulus of block; and E_c is the elastic modulus of composite block.

Determination of Mortar Layer Cohesive-element Parameters

The zero-thickness cohesive contact model considering friction was used to simulate the mortar layer, while the “traction separation model” in ABAQUS was used to explain the relationship between interface tensile stress, shear stress and interface relative displacement. The traction separation model is linear elastic at the initial stage. After the ultimate strength is exceeded, the interfacial strength begins to decrease. The degradation behavior of the mechanical properties can be simulated using the initial damage and damage evolution laws. Quad damage was selected as the damage model and damage evolution was defined simultaneously.

The values of the mortar normal interface stiffness k_n and two tangential interface stiffnesses k_s and k_t were determined based on a previous study (Aref and Dolatshahi, 2013) and calculated according to Eqs. (8) and (9).

$$k_\mathrm{n} = \frac{1}{h_\mathrm{m}} \frac{E_\mathrm{m} E_\mathrm{b}}{E_\mathrm{b} - E_\mathrm{m}} \quad (8)$$

$$k_\mathrm{s} = k_\mathrm{t} = \frac{1}{h_\mathrm{m}} \frac{G_\mathrm{m} G_\mathrm{b}}{G_\mathrm{b} - G_\mathrm{m}} \quad (9)$$

Here, G_b and G_m are the shear modulus of the block and mortar, respectively. The shear modulus is calculated according to the Poisson's ratio and elastic modulus and the Poisson's ratio of the block and mortar is taken as 0.15. h_m is the thickness of the mortar layer and the thickness of the mortar layer is 10mm for calculation.

The damage constitutive model of the interface includes two stages; damage initiation and damage evolution. The secondary stress criterion is used as the damage generation criterion, as in Eq. (10).

$$\left(\frac{t_\mathrm{n}}{t_\mathrm{n}^0}\right)^2 + \left(\frac{t_\mathrm{s}}{t_\mathrm{s}^0}\right)^2 + \left(\frac{t_\mathrm{t}}{t_\mathrm{t}^0}\right)^2 = 1 \quad (10)$$

Here, t_n^0, t_t^0 and t_s^0 are the ultimate traction forces in the online elastic stage of the traction separation model. In this study, the traction force was calculated according to Eqs. (11) and (12) (Jiang and Zhou, 2019).

$$t_\mathrm{n}^0 = 0.1 f_\mathrm{m} \quad (11)$$

$$t_\mathrm{s}^0 = t_\mathrm{t}^0 = 2 \times 0.125\sqrt{f_\mathrm{m}} \quad (12)$$

The damage factor D is used to express the degree of damage. Its initial value is 0 and it is 1 when the damage is complete. The evolution criterion of energy is adopted and the fracture energy is used to describe the damage factor D. The softening mode is exponential and the softening behavior is defined by the Benzeggagh-Kenane criterion, as shown in Eq. (13). The fracture energy is the total area under the traction separation curve.

$$G^C = G_n^C + \left(G_s^C - G_n^C\right)\left(\frac{G_S}{G_T}\right)^{\alpha} \tag{13}$$

Here, G_n^C is the critical fracture energy of failure in the normal direction of the contact surface; G_s^C is the critical fracture energy of failure in the first shear direction of the contact surface; G_S is the sum of the fracture energy in the two shear directions of the contact surface during the loading process; G_T is the sum of the fracture energy in the shear direction during loading; G^C is the sum of the fracture energy in the normal direction and shear direction of the contact surface during the loading process; α is the BK index, which is taken as 2.0 in this paper.

According to the tests by Dolatshahi and Aref (2011) and Mohammed (2010), the normal and tangential fracture energies are estimated according to the calculated values of the interface tensile and shear strengths, as shown in Eq. (14).

$$G_n^C\left(G_s^C\right) = G_{n,\ test}^C\left(G_{s,\ test}^C\right)\frac{t_n^0\left(t_s^0\right)}{t_{n,\ test}^C\left(t_{s,\ test}^0\right)} \tag{14}$$

Here, $t_{n,\ test}^0$ = 0.25MPa and $t_{s,\ test}^0$ = 0.35MPa, respectively, representing the normal strength and tangential strength of masonry obtained from relevant tests; whereas $G_{n,\ test}^C$ = 18N/m and $G_{s,\ test}^C$ = 125N/m, respectively, representing the normal fracture energy and tangential fracture energy of masonry obtained from relevant tests.

Because of the poor plumpness and bond strength of the vertical mortar joint, its strength and fracture energy are generally taken as 0.5 times those of the horizontal mortar joint.

Modeling and Verification of Finite-element Model of Masonry Wall

Establishment of Finite-element Model of Wall

Based on the masonry wall test as the background, a finite-element model of the separated masonry wall was established for low-cycle loading simulation. The W02 wall in a study (Jiang et al., 2019) was selected as the research object and the wall size was 2100 × 1560 × 240 mm (length × width × thickness), a single brick size was 240 × 115 × 53 mm (length × width × thickness), as shown in Figure 2. The masonry materials were M5 mortar (measured compressive strength of 1.19 MPa) and MU10 clay brick (measured compressive strength of 12.66 MPa). The parameters of the block and mortar layers were calculated according to the above-mentioned parameter calculation process. Some of the parameters are listed in Table 1. The concrete loading beam and ground beam were set with a large elastic modulus to ignore their deformation.

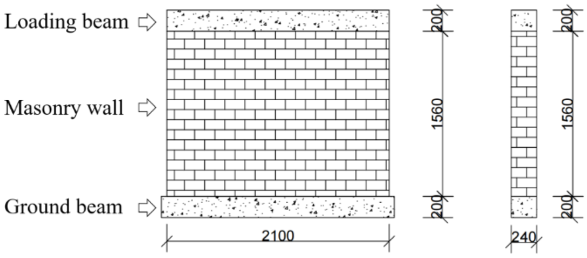

Figure (2): Dimensional drawing of masonry wall

Table 1. Partial calculation parameters of separated wall

Elastic Modulus (MPa)		Parameters of mortar layer of horizontal mortar					
		IS (10^{10}N/m^3)		FE (N/m)		UT (MPa)	
Mortar	Brick	K_{nn}	$K_{ss} = K_{tt}$	G_n^c	$G_s^c = G_t^c$	t_n^0	$t_s^0 = t_t^0$
532	1058	145.00	63.00	0.0111	0.0974	0.154	0.2730

IS, Interface Stiffness; FE, Fracture Energy; UT, Ultimate traction.

The composite block and concrete beam were simulated using a solid element (C3D8R) and a zero-thickness cohesive element (COH3D8) was inserted at the joint of the block to simulate the mortar layer, as shown in Figure 3. The normal "hard" contact and tangential friction contact were set and the friction coefficient was taken as 0.75 (Ding et al., 2015).

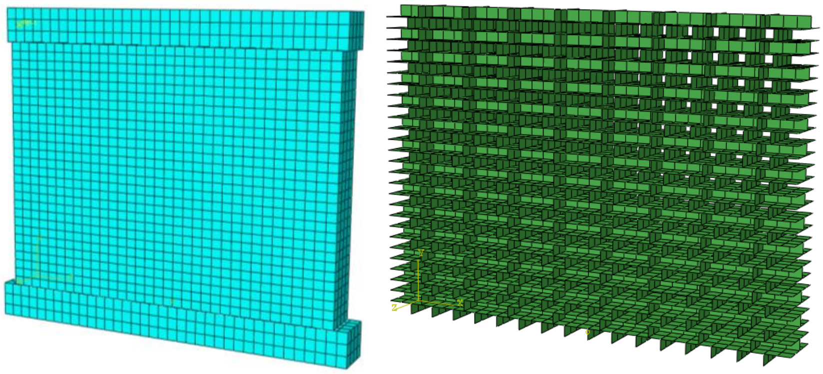

(1) Finite element model of wall (2) Element of mortar layer

Figure (3): Finite element model of wall and mortar layer

To coordinate the deformation, the upper end of the wall was connected to the loading beam and the lower end was connected to the ground beam. A fixed boundary was set on the bottom surface of the ground beam and a 0.516-MPa vertical pressure was applied to the surface of the upper loading beam. The loading beam surface was coupled to point RP-1. The displacement amplitude was increased by 1.2 times that of the previous step and the *X*-direction displacement was loaded at RP-1 on the side of the loaded beam. The display dynamics were selected in the analysis step and the effect of cell deletion was set. The finite-element wall loading setting is shown in Figure 4.

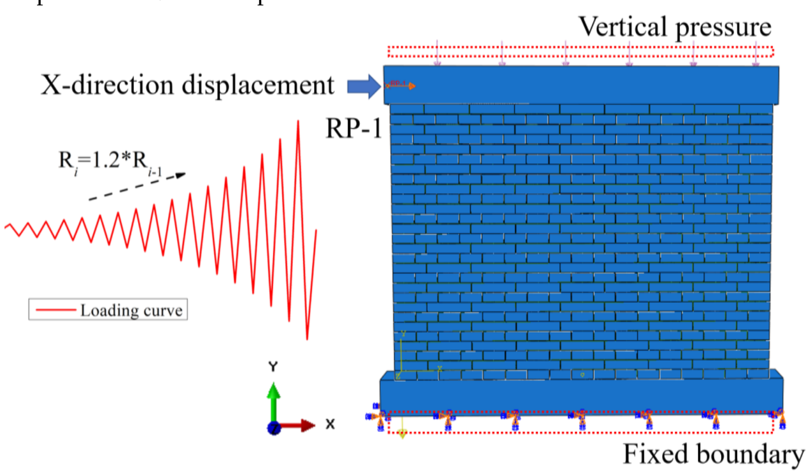

Figure (4): Loading diagram of wall model

To observe the damage and deletion effects of the cohesive element in the postprocessing stage, it was necessary to set the corresponding parameters in the field variable output and select SDEG, DMICRT and STATUS.

Reliability Verification of Finite-element Model of Masonry Wall

At the beginning of loading, with an increase in the horizontal displacement to 1.09 mm, cracks first appear in the middle and lower parts of the wall. When the horizontal displacement increases to 4.15 mm, the peak load reaches 138.56 kN. When the wall is damaged after subsequent loading, several inclined cracks appear in the brick masonry wall and run along the wall. The inclined cracks expand into type-X cracks. The corresponding diagrams of the final failure of the test and simulated wall are shown in Figure 5.

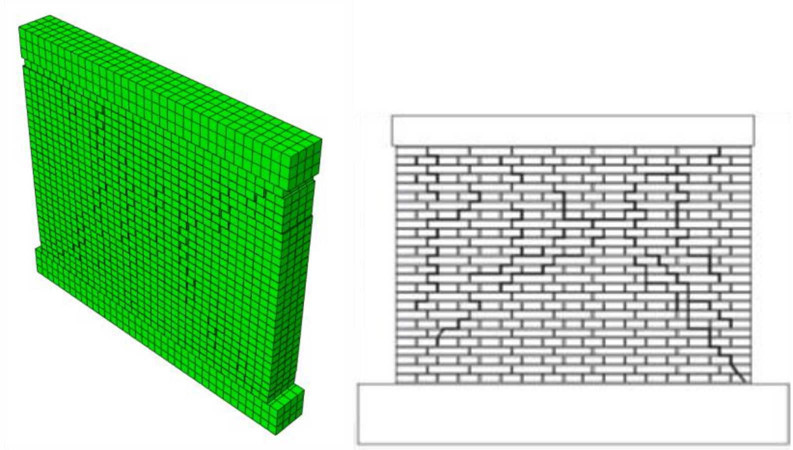

(a) Simulated crack form (b) Test crack form(Jiang et al., 2019)

Figure (5): Comparison between simulated and test wall cracks

The skeleton curve of the masonry wall obtained by simulation was compared with the test results. As shown in Figure 6, the overall shapes of the two skeleton curves are relatively close. The test results, numerical simulation results and deviations are summarized in Table 2.

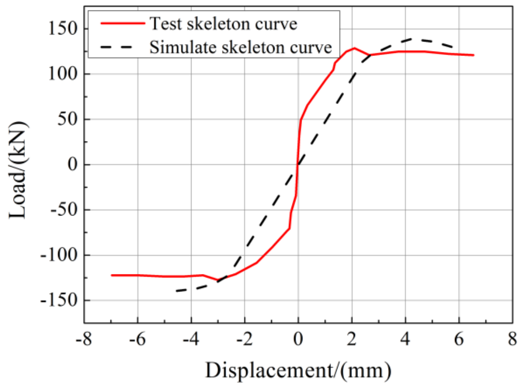

Figure (6): Skeleton curve of masonry wall obtained from test and simulation

Table 2. Comparison of test and simulation results of masonry wall

	CL (kN)	CD (mm)	PL (kN)	PD (mm)	CDL (kN)	CDD (mm)
(Jiang et al., 2019)	98.70	1.13	128.90	2.61	109.60	9.00
Simulaiton	76.50	1.09	138.56	4.15	106.00	7.13
Deviation	-22.50%	-3.50%	-6.97%	59.00%	-3.28%	-20.70%

C, Cracking load; D, displacement, P, Peak; L, Load; CD, Collapse damage.

The simulation results are similar to the experimental results, except for the peak displacement. In the simulation, the damage evolution was set for the model mortar layer. When the damage reaches the set parameter 1, the mortar layer performance declines. However, in the test, the failure point of the mortar layer was not absolute. Therefore, the simulation error of the peak displacement is relatively large. Nevertheless, the simulation method used in this study is reliable overall and can accurately reflect changes in wall shear capacity, crack development and mortar damage.

Effect of Long-term Immersion on the Shear Capacity of Masonry Wall

Simulation Parameters of Long-term Immersion Masonry Wall

Flooding affects mechanical properties of cement materials. During flood disasters, the extreme case of house immersion time can last for more than one month. Jing et al. (2017) found that the compressive strength of mortar and clay bricks tended to be stable after long-term immersion; therefore, the conservative residual strengths of the clay brick and mixed mortar were determined, as calculated according to Eqs. (15) and (16).

$$f_{1,\mathrm{res}} = 0.73 f_{\mathrm{b}} \tag{15}$$

$$f_{2,\mathrm{res}} = 0.55 f_{\mathrm{m}} \tag{16}$$

Here, $f_{1,\mathrm{res}}$ is the conservative residual strength value of the brick in a wet state after long-term immersion and $f_{2,\mathrm{res}}$ is the conservative residual strength of the mixed mortar in a wet state after long-term immersion.

The above equations provide the strength reduction for the deterioration of mortar and brick. At the same time, flood immersion can also affect the bonding performance of brick masonry. In the saturated moisture content state, the normal bond strength of the masonry decreased by approximately 40%. The shear strength of the brick masonry decreased by more than 50% after long-term immersion (Zhao et al., 1997). Therefore, in this study, a reduction calculation was performed when simulating the traction force parameters of the mortar layer viscous element of the immersed masonry wall, as shown in Eqs. (17) and (18).

$$t'_{\mathrm{n}} = 0.5 \times 0.1 f_{2,\mathrm{res}} \tag{17}$$

$$t'_{\mathrm{s}} = t'_{\mathrm{t}} = 0.4 \times 2 \times 0.125 \sqrt{f_{2,\mathrm{res}}} \tag{18}$$

Here, t'_{n} is the normal traction force of the immersed masonry wall and t'_t is the tangential traction force of the immersed masonry wall.

For the simulation in the wet state, the friction coefficient is taken as 0.6 for simulation in wet state (Code for design of masonry structures (GB 50003-2011), 2011). The wall modeling process and loading settings are the same as those described above.

Comparison of Shear Performance of Masonry Wall after Immersion

The hysteretic and skeleton curves of the masonry wall after immersion obtained from the simulation were compared, as shown in Figures 7(a) and 7(b). The wall stiffness was calculated according to Eq. (19) and normalized. The changes in stiffness are shown in Figure 7(c).

$$K_i = \frac{|F_i| + |-F_i|}{|\Delta_i| + |-\Delta_i|} \tag{19}$$

Here, $+F_i$ and $-F_i$ are the loads at the peak point of the *i* times reciprocating load, respectively; $+\Delta_i$ and $-\Delta_i$ are the displacements of the peak point of the *i* times reciprocating load, respectively.

The crack development pattern and mortar damage nephogram of the immersed wall are shown in Figures 8(a) and 8(b), respectively.

Comparing the skeleton and stiffness curves revealed that the shear performance of a masonry walls changes significantly after long-term flood immersion. After immersion, the ultimate shear capacity of the masonry wall was reduced by 44.26 kN, a decrease of 31.73%. The damage displacement increased compared with the original wall. When the masonry wall reached the ultimate load, its strength decreased slowly and was almost flat. After immersion, the strength of the material decreased and the initial stiffness of the wall was much lower than that of the original wall. During the loading process, the stiffness decreased gradually; however, this change was not significant. The observation of wall cracks and mortar layer damage shows that the cracks in the immersed wall developed more seriously when the wall was damaged and almost all mortar units ceased working. At that time, the bearing function was mainly performed by the friction between the materials.

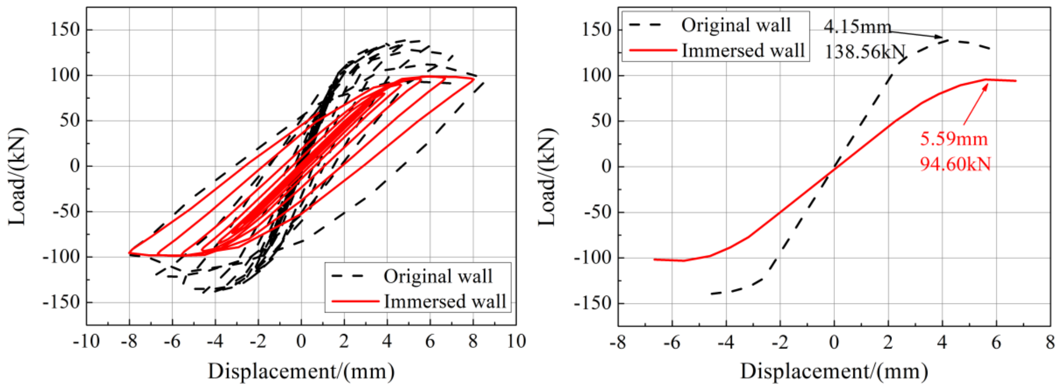

(a) Comparison of hysteresis curves (b) Comparison of skeleton curves

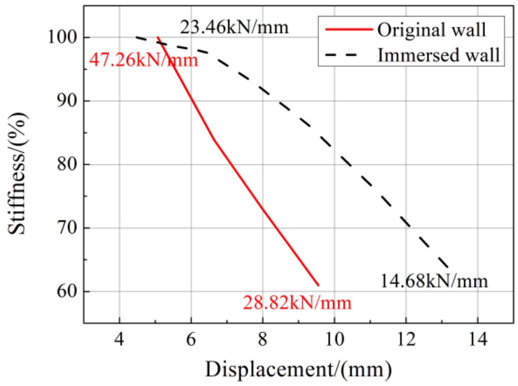

(c) Comparison of masonry wall stiffness changes

Figure (7): Comparison of mechanical parameters between original and immersed walls

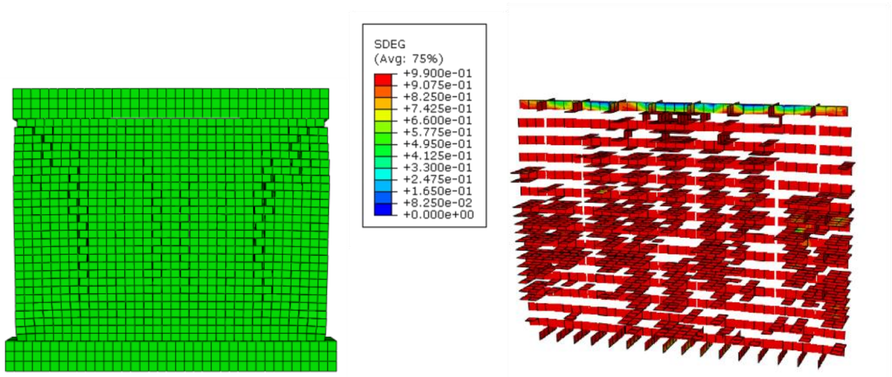

(a) Crack pattern of immersed wall (b) Damage of immersed wall mortar

Figure (8): Damage to immersed wall

The immersed masonry wall exhibited a low bearing capacity and low stiffness. The wall mortar and bonding performance decreased significantly and the shear performance was mainly provided by friction. The shear capacity of the immersed wall was clearly insufficient and a safety reserve could not be guaranteed. This phenomenon may be more prominent in single-layer masonry buildings with low vertical pressure.

Effect of Partial Immersion on Shear Performance of Masonry Wall

A finite-element model of a partially immersed masonry wall was established. The range of influence of the immersion was set to a half of the wall height and the material properties of the corresponding parts were changed. The modeling process and loading settings were the same as those described above.

The skeleton curve of the partially immersed wall was compared with that of the original wall, as shown in Figure 9.

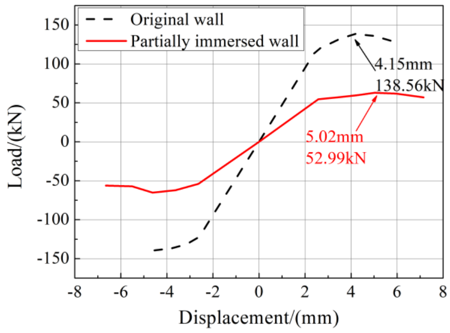

Figure (9): Comparison of skeleton curves

As Figure 9 shows, the difference between the skeleton curve of the partially immersed wall and that of the original wall is obvious. Taking the original wall as the initial state, the ultimate shear capacity of the partially immersed wall was reduced by 85.57 kN, with a decrease rate of 61.75%, indicating significant danger.

The crack development pattern and mortar damage cloud diagram of the wall at the time of failure are shown in Figures 10(a) and 10(b), respectively.

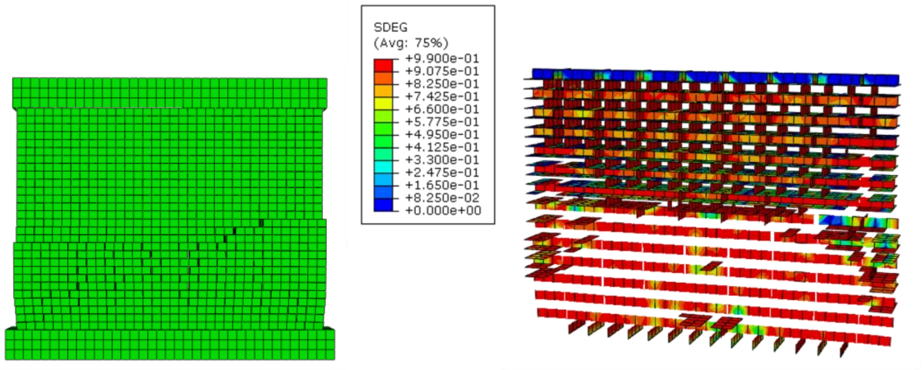

(a) Crack pattern (b) Damage of wall mortar

Figure (10): Damage to partially immersed wall

The cracks in the lower wall developed more significantly. Partial sliding occurred in the middle of the wall and the failure mode changed. According to the analysis of mortar damage, part of the immersed wall had serious damage and almost all failures occurred during the loading process. This was because the mortar strength and bonding performance of the lower part of the wall were far lower than those of the upper wall. The mortar on the upper wall was less damaged and did not participate fully in the loading process. These results demonstrate that some immersed walls may be damaged from the weak parts and the shear capacity decreases significantly, indicating greater risk.

Analyzing the Damage of Masonry Wall by Crack Width

Extracting Crack Width Data of Masonry Wall Model

Reflecting the degree of damage to a masonry structure using the interlayer displacement angle is difficult. As a typical apparent physical index of a building structure, the crack width reflects the safety state and degree of damage of a structure. To analyze the change in crack width in the simulation process of a separated masonry wall, the ABQUAS postprocessing results were processed using Python to extract the crack width data.

Among the three groups of opposites in the cohesive element, only the normal opposites can be separated from each other and the separation direction is defined as the thickness direction. In the eight-node element, the top surface is defined by the first four nodes, while the bottom surface is defined by the last four nodes. The thickness direction is from bottom to top and the distance between the top and the bottom of the unit can be considered the crack width, as shown in Figure 11.

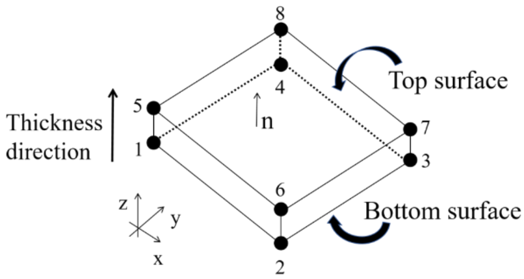

Figure (11): Diagram of thickness direction of cohesive element

Comparison of Masonry Wall Crack Width Change and Damage

Using the above method, the change curve of the crack width with time during the loading process of the original and immersed masonry walls was extracted and the residual crack width data is depicted in Figure 12.

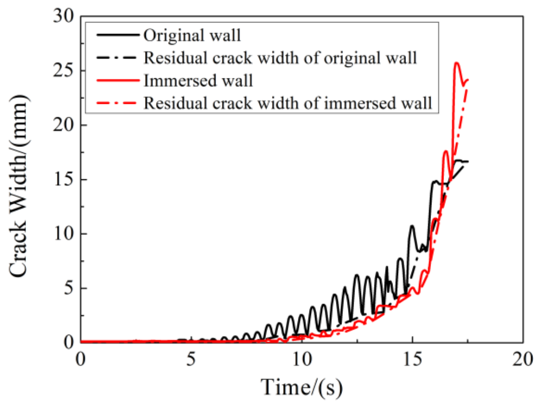

Figure (12): Variation of crack width of masonry wall

According to the change in crack width, the cracks in the original wall appear to open and close repeatedly with reciprocating loading. However, the wall is prone to permanent cracks after immersion and this does not change significantly with reciprocating loading. During development, the crack width of the immersed wall is smaller than that of the original wall. When the load reaches the failure stage, the crack width of the immersed wall suddenly increases, forming a residual crack significantly wider than that of the original wall.

Jiang et al. (2018) analyzed the relationship between the interlayer displacement angle and the macro-damage degree (crack width) of a masonry structure. Su et al. (2013) determined that the limit value of the interstory displacement angle for the collapse of a masonry structure is 1/150.

The crack widths corresponding to the interlayer displacements of the corresponding failure levels during wall loading are listed in Table 3.

Table 3. Crack width of masonry wall corresponding to different damage grades

Damage grade	**Inter-story displacement angle**	**Crack width limit/mm (Jiang et al., 2018)**	**Crack width of original wall/mm**	**Crack width of immersed wall/mm**
Basically intact	1/1000	0.1	0.49274	0.13944
Minor damage	1/670	1.0	1.647	0.6555
Moderate damage	1/330	5.0	5.0	1.4
Serious damage	1/165	10.0	14.6	11.28
Collapse damage	1/150	/	16.66	24.16

From the performances of the two wall crack widths in Table 4, when the interlayer displacement of each damage grade is loaded, the crack width of the original masonry wall at each stage is equal to or greater than the corresponding relationship in Table 3 and the crack width has the function of failure early warning. The crack width of the immersed wall before the serious damage stage is lower than the crack width corresponding to the degree of damage and is smaller than that of the original wall as a whole. However, when the loading reaches the collapse stage, the crack width of the immersed wall suddenly increases and becomes much larger than that of the original wall. Therefore, the macro-damage degree of the immersed masonry wall is not as serious as that of the original wall in the early stage; however, it is prone to sudden collapse damage and the early warning effect of cracks is reduced, which requires special attention in safety appraisal.

CONCLUSIONS

(1) A cohesive element considering contact was used to simulate the mortar layer and the damage evolution of the cohesive element was defined. A finite-element model of a separated masonry wall was established for numerical low-cycle loading simulation. A comparison between the simulation results and previous test results proves that the simulation method can reliably show the development of cracks and the damage to the mortar layer.

(2) Long-term flood immersion affects the strength

properties of masonry materials and the bonding performance of mortar. After immersion, the masonry wall exhibited a low bearing capacity and a low stiffness. Most of the mortar layers failed in the late loading stage and the shear performance was mainly provided by friction. The shear bearing capacity of the wall after immersion was insufficient and its safety reserve could not be guaranteed.

(3) The mortar strength and bonding performance of the partially immersed wall decreased. The soaked part of the wall was severely damaged during the loading process and almost all of it failed. The mortar in the unimmersed part of the wall was less damaged and did not fully participate in the loading. Some immersed walls may be damaged from weak positions, indicating great danger.

(4) After processing the ABQUAS software post processing data using Python, the change data of the crack width of the masonry wall with time was defined and extracted. The analysis of the crack width and damage degree shows that the macro-damage degree of the immersed masonry wall was not as serious as that of the original wall in the early stage and was lower than the crack width limit of the corresponding damage degree; however, it could suddenly reach the collapse damage degree. The early warning effect of cracks was reduced, requiring special attention during safety appraisals.

Declaration of Competing Interests

The authors declare that they have no known or potential competing financial interests or personal relationships that could have appeared to influence the work reported in this paper.

Acknowledgement

We would like to thank Editage (www.editage.cn) for English-language editing.

Funding

This work was supported by National Key R&D Program of China (2022YFC3003505).

REFERENCES

Aref, A.J., and Dolatshahi, K.M. (2013). “A three-dimensional cyclic meso-scale numerical procedure for simulation of unreinforced masonry structures”. Computers & Structures, 120 (15), 9-23.

Chen, Y., Liu, T., Ge, Y. et al. (2021). “Examining social vulnerability to flood of affordable housing communities in Nanjing, China: Building long-term disaster resilience of low-income communities”. Sustainable Cities and Society, 71, 102939.

Ding, R.B., Zhang, W.F., and Niu, L.J. (2015). “Numerical simulation of masonry shear bearing capacity in compression-shear”. Construction Technology, 44 (S2), 588-592 (in Chinese).

Dolatshahi, K.M., and Aref, A.J. (2011). “Two-dimensional computational framework of meso-scale rigid and line interface elements for masonry structures”. Engineering Structures, 33 (12), 3657-3667.

Dong, Z.Q., Li, G., Song, B. et al. (2022). “Failure risk assessment method of masonry structures under earthquakes and flood scouring”. Mechanics of Advanced Materials and Structures, 29 (21), 3055-3066.

Drucker, D.C., and Prager, W. (1952). “Soil mechanics and plastic analysis or limit design”. Quarterly of Applied Mathematics, 10 (2), 157-165.

Franzoni, E., Gentilini, C., Graziani, G. et al. (2015). “Compressive behaviour of brick masonry triplets in wet and dry conditions”. Construction and Building Materials, 82 (1), 45-52.

Haddad, R., and M. Jamal, S. (2008). “Performance of Jordanian masonry cement for construction purposes”. Jordan Journal of Civil Engineering, 2 (1), 20-31.

Jiang, J.T., and Zhou, X.Z. (2019). “Discussion on parameters in finite element analysis of mechanical properties of masonry wall based on separation modeling”. Building Structure, 49 (S1), 640-644 (in Chinese).

Jiang, J.T., Rao, G.D., Zhou, X.Z. et al. (2019). “Single wall pseudo-static experimental research of steel bar-mortar layer crossed strip method for reinforcement of existing masonry wall”. Building Structure, 49 (05), 17-22 (in Chinese).

Jiang, L.X., Wang, Z.L., and Zhang, F.W. (2018). “Damage degree and inter-story drift angle limit of multi-story masonry structures”. Journal of Building Structures, 39 (S2), 263-270 (in Chinese).

Jing, D.H., Cao, S.Y., and Chen, H. (2017). "Axial compression performance investigation of brick masonry after being long-term soaked in water and air-dried". Sichun Building Science, 43 (02), 29-32 (in Chinese).

Kaushikm, H.B., Rai, D.C., and Jain, S.K. (2007). "Stress-strain characteristics of clay brick masonry under uniaxial compression". Journal of Materials in Civil Engineering, 19 (9), 728-739.

Kong, J.C., Zhai, C.H., Li, S. et al. (2012). "Study on in-plane seismic performance of solid masonry- infilled RC Frames". China Civil Engineering Journal, 45 (S2), 137-141 (in Chinese).

Kujawa, M., Lubowiecka, I., and Szymczak, C. (2020). "Finite element modeling of a historic church structure in the context of a masonry damage analysis". Engineering Failure Analysis, 107, 104233.

Liu, G.Q., Shi, C.X., and Liu, Y.B. (2008). "Analyses of the elastic modulus values of masonry". Journal of Hunan University (Natural Sciences), 35 (04), 29-32 (in Chinese).

Ministry of Housing and Urban-Rural Development of the People's Republic of China. (2011). "Code for design of masonry structures (GB 50003-2011)". Beijing:China Architecture and Building Press (in Chinese).

Mohammed, M. (2010). "Finite element analysis of unreinforced masonry walls". Al-Rafidain Engineering Journal, 18 (4), 55-68.

Pandey, A.K, and Bisht, R.S. (2014). "Numerical modeling of infilled clay brick masonry under blast loading". Advances in Structural Engineering, 17 (4): 591-606.

Sathiparan, N., and Udayakumar, R. (2018). "Effect of moisture condition on mechanical behavior of low strength brick masonry". Journal of Building Engineering, 17, 23-31.

Song, B., Lu, C.H., Wang, M.S. et al. (2023). "Aseismic effect of old single-layer masonry agricultural house structure strengthened with embedded steel frame and steel strip". Canadian Journal of Civil Engineering, 50 (9), 804-813.

Su, Q.W., Xu, H., Wu, H. et al. (2013). "Research on inter-story displacement angle of brick masonry structures". China Civil Engineering Journal, 46 (S1), 111-116 (in Chinese).

Zeng, B, Li, Y., and Noguez, C.C. (2021). "Modeling and parameter importance investigation for simulating in-plane and out-of-plane behaviors of unreinforced masonry walls". Engineering Structures, 248, 113233.

Zhao, K.C., Wang, X.P., Fu, C.G. et al. (1997). "Experimental study of the behavior of brick wall soaked in water". Journal of Building Structures, 18 (01), 27-32 (in Chinese).

Zhao, Z., Dai, Z.C., Zhong, X.G. et al. (2021). "A two-phase modeling method based on cohesive elements for masonry arches". Engineering Mechanics, 38 (12), 97-106, 117 (in Chinese).